Preprints of the 21st IFAC World Congress (Virtual)
Berlin, Germany, July 12-17, 2020

Multivariable Dynamic Input Shaping for Two-Axis Fast Steering Mirror

Alicia Dautt-Silva * **Raymond A. de Callafon** **

* *University of California San Diego, La Jolla, CA 92093-0411 USA (e-mail: adauttsi@eng.ucsd.edu).*
** *University of California San Diego, La Jolla, CA 92093-0411 USA (e-mail: callafon@ucsd.edu)*

Abstract: A two-axis Fast Steering Mirror (FSM) is a commonly used mechanical component used in optical imaging and laser beam steering. This paper shows how inverse kinematic analysis and dynamic input shaping can be used to compute the two-axis input signals for the actuation of a FSM to be able to track a desired output trajectory. The approach is based on quasi-static kinematic analysis and dynamic modeling of a two-axis FSM multivariable motion from experimental step response data. It is shown how open-loop tracking can be improved by properly designed dynamic input shaping signals that take into account the inverse kinematics and dynamic response of the FSM.

Keywords: fast steering mirror; kinematics; step-response; identification; input shaping.

1. INTRODUCTION

A Fast Steering Mirror (FSM) is a commonly used mechanical component in optical applications, such as astronomy, laser beam pointing systems, laser communication, opthalmology and laser cutting (Chen et al., 2010). The analysis of how a laser propagates from the beam source via a mechanically adjustable mirror to a target is part of a multidisciplinary problem called "beam control" as described by Merritt and Spencer (2018). Accuracy of beam steering is influenced by mechanical coupling, hysteresis and dynamics of the mirror itself (Zhu et al., 2015), but also by atmospheric conditions in case of long-distance pointing (Roggemann and Welsh, 1996). Innovative approaches such as real-time or adaptive control of mirrors (Kim et al., 2004) can greatly improve the accuracy of beam steering, but require real-time measurements of the beam target location.

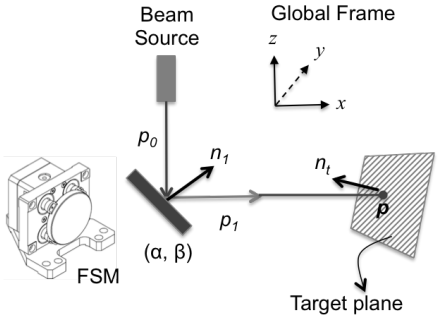

Fig. 1. Beam and steering mirror system

Following the schematic description on Fig. 1, this paper presents an open-loop approach to compute optimal steering signals of a FSM controlled by a Voice Coil Motor (VCM) on each axis to achieve a desired trajectory in a target plane. The VCM actuation of the FSM ensures minimal hysteresis effects, unlike the use of piezo-stacks for FSM actuation, discussed in Zhu et al. (2015). Furthermore the proposed open-loop approach in this paper uses experimental data of the dynamic response of the FSM to formulate the optimal input shaping signals. Although detailed dynamic modeling of mirror dynamics is useful for analysis and design in high precision mirror systems (Schitter et al., 2008), it is shown that a reliable realization method presented in de Callafon and Miller (2012) can be used to directly formulate a linear multivariable dynamic model that captures the coupled dynamics of the two-axis VCM actuation of the FSM. Recent approaches of data-based input shaping have been recognized for input shaping of mechanical or MEMS devices, see e.g. Kim et al. (2019), but often ignore the possible dynamic coupling effects in case of multi-axis actuation as seen in a FSM.

The input shaping for a two-axis FSM is broken down in two separable parts in this paper. The first part consists of the forward kinematics and dynamic analysis of the FSM. The forward kinematics uses the reflection matrix or mirror transformation matrix as defined in DeBruin and Johnson (1992) to describe the quasi-static behavior of the beam reflection as a function of the two-axis rotation of FSM based on the work by Hilkert et al. (2014) and Merritt and Spencer (2018). Dynamic analysis of the FSM is based on step-response experiments that measure the dynamic response of the two-axis rotation of FSM and formulate a linear multivariable discrete-time dynamic model based on the realization algorithm described in de Callafon and Miller (2012).

The second part consists of the inverse kinematic analysis of the FSM, along with the computation of a set of dynamic voltage inputs to the VCMs used to steer the FSM. The inverse kinematics computes the desired quasi-static movement of the FSM from a desired target trajectory parametrization for beam forming. The set of

dynamic voltage inputs to the VCMs of the FSM are solved by a Linear Programming (LP) problem similar to Dautt-Silva and de Callafon (2018) but extended to the multivariable situation of the FSM. The LP problem uses the multivariable model to solve the input assignment under constraints to find a feasible solution for the input shaping of the FSM. Results are illustrated by the tracking of a square target reference to show the effectiveness of the proposed multivariable input shaping.

2. MIRROR BEAM-POINTING KINEMATICS

2.1 Rotated normal of the mirror

For the kinematic analysis we consider the steering mirror in Fig. 2, whose rotation axes are located at the center of the mirror. The reflection problem of a beam by the mirror can be expressed as a matrix multiplication,

$$p_1 = Tp_0, \tag{1}$$

where T denotes the reflection matrix and p_0 and p_1 represent unit vectors in the directions of the incident beam and reflected beam, respectively. Following the approach of Hilkert et al. (2014), we will write the reflection matrix T as a function of the rotation of the normal vector n of the mirror plane to accommodate inverse kinematic analysis.

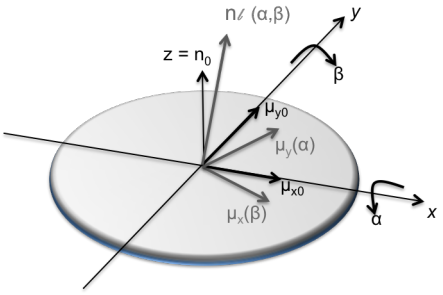

Fig. 2. Steering mirror axes and normal

Without loss of generality, the local mirror frame is defined to be the x- and y-axes in the plane of the mirror and the normal n_0 is aligned with the a z-axis. The mirror can be rotated about both its x- and y-axes independently by the angles α and β, changing and the normal vector n of the mirror as follows. With the unit vectors

$$\mu_{x0} = [1\ 0\ 0]^T\ ,\ \mu_{y0} = [0\ 1\ 0]^T$$

in the local mirror frame and the Euler transform (or rotation) matrices

$$R_x(\alpha) = \begin{bmatrix} 1 & 0 & 0 \\ 0 & \cos\alpha & -\sin\alpha \\ 0 & \sin\alpha & \cos\alpha \end{bmatrix},\ R_y(\beta) = \begin{bmatrix} \cos\beta & 0 & \sin\beta \\ 0 & 1 & 0 \\ -\sin\beta & 0 & \cos\beta \end{bmatrix}$$

based on the rotation angles α and β, the rotated unit vectors of the normal are given by

$$\mu_x(\beta) = R_y(\beta)\mu_{x0} = \begin{bmatrix} \cos\beta \\ 0 \\ -\sin\beta \end{bmatrix}, \tag{2}$$

$$\mu_y(\alpha) = R_x(\alpha)\mu_{y0} = \begin{bmatrix} 0 \\ \cos\alpha \\ \sin\alpha \end{bmatrix}. \tag{3}$$

As a result, the normal of the mirror $n_\ell(\alpha,\beta)$ in the local mirror frame is obtained with the cross product $n_\ell(\alpha,\beta) = \mu_x(\beta) \times \mu_y(\alpha)$ and leads to

$$n_\ell(\alpha,\beta) = \begin{bmatrix} \cos\alpha\sin\beta \\ -\cos\beta\sin\alpha \\ \cos\beta\cos\alpha \end{bmatrix}. \tag{4}$$

The normal $n_\ell(\alpha,\beta)$ of the mirror in the local mirror frame must be referenced to the global frame by considering the mounting angle of the mirror. The angle of rotation of the mirror relative to the global frame can again be described by a rotation around the x- and y- and z-axis of the global frame with rotation matrices $R_x(\phi)$, $R_y(\theta)$ and $R_z(\psi)$ defined by the matrices

$$\begin{bmatrix} 1 & 0 & 0 \\ 0 & \cos\phi & -\sin\phi \\ 0 & \sin\phi & \cos\phi \end{bmatrix},\ \begin{bmatrix} \cos\theta & 0 & \sin\theta \\ 0 & 1 & 0 \\ -\sin\theta & 0 & \cos\theta \end{bmatrix},\ \begin{bmatrix} \cos\psi & -\sin\psi & 0 \\ \sin\psi & \cos\psi & 0 \\ 0 & 0 & 1 \end{bmatrix}$$

respectively. As a result, the rotated normal of the mirror in global frame is given by

$$n(\phi,\theta,\psi,n_\ell(\alpha,\beta)) = R_x(\phi)R_y(\theta)R_z(\psi)n_\ell(\alpha,\beta) \tag{5}$$

where the normal $n(\cdot)$ in (5) is now also a function of the rotation angles (ϕ,θ,ψ) and the normal of the mirror n_ℓ in (4). With the mounting angles (ϕ,θ,ψ) all fixed, the rotation matrices can be characterized as constant, making

$$n(\alpha,\beta) = R\,n_\ell(\alpha,\beta) \tag{6}$$

with $n_\ell(\alpha,\beta)$ defined in (4) and $R = R_x(\phi)R_y(\theta)R_z(\psi)$.

2.2 Beam reflection

With the rotated normal $n(\alpha,\beta)$ given in (6), Fig. 3 shows an incident beam p_0 and the reflected beam p_1. It should be noted that p_0 and $n(\alpha,\beta)$ span the beam plane and the reflected beam lies in the same beam plane, due to the assumption of a flat mirror.

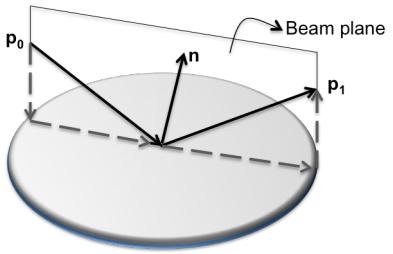

Fig. 3. Incident and reflected beam decomposition

With the notion of a perpendicular component $p_{1\perp}$ and parallel component $p_{1\|}$ (Hilkert et al., 2014), it is clear that $p_1 = p_{1\perp} + p_{1\|} = p_{0\perp} - p_{0\|}$ and

$$p_1 = p_0 - 2p_0 n(\alpha,\beta)n^T(\alpha,\beta),$$

which can be rewritten in the simplified matrix form $p_1 = T(n(\alpha,\beta))p_0$ as mentioned earlier in (1). The analysis reveals that the reflection matrix $T(n(\alpha,\beta))$ is given by

$$T(n(\alpha,\beta)) = I_3 - 2n(\alpha,\beta)n^T(\alpha,\beta) \tag{7}$$

in terms of the normal vector $n(\alpha,\beta)$ of the mirror.

It should be noted that if the mirror is kept in a fixed position, the normal $n(\alpha,\beta)$ and the reflection matrix $T(n(\alpha,\beta))$ are constant, making the direction p_1 of the reflected beam only a function of the direction p_0 of the incident beam. Vice versa, keeping the incident beam direction fixed at p_0, the direction p_1 of the reflected beam can be adjusted by varying the rotation angle pair (α,β) of the mirror. In this case, the reflection matrix $T(n(\alpha,\beta))$ varies as function of the mirror rotation.

2.3 Beam intersection point

As the reflected beam p_1 leaves the mirror, it creates a target location on a subsequent target plane. This plane could be an imaging surface or another secondary mirror, as indicated in Fig. 4.

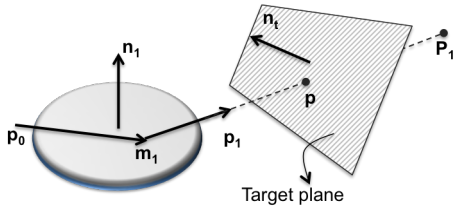

Fig. 4. Reflected beam intersection with the target plane

Consider the reflected beam with a direction vector p_1, start point m_1, and a final point P_1 which is derived from the previous values. We have the segment $\overline{m_1 P_1}$ and following O'Rourke (1998) we derive the intersection point.

$$P_1(m_1, p_1) = m_1 + k d p_1^T, \tag{8}$$

where k is a scale factor to assure the segment will be longer than the distance d to the plane. The distance d is a constant value known based on the opto-mechanical layout.

The intersection p with the plane is derived with the parametric line equation

$$p(m_1, P_1, n_t) = m_1 + s \times (P_1 - m_1), \tag{9}$$

where n_t is the normal of the subsequent plane and s is the intersection parameter scalar obtained as

$$s = \frac{n_t \cdot (m_1 - p_t)}{n_t \cdot (P_1 - m_1)}. \tag{10}$$

3. MIRROR ROTATION DYNAMICS

3.1 Step response excitation

A fast steering mirror (FSM) typically consists of a mirror, polished and with coatings such as protected gold, aluminum or silver, Merritt and Spencer (2018). Precision movement of the FSM is done via embedded actuators capable of rotating the mirror closely along its two perpendicular axes that typically intersect on the center of the mirror (Zhou et al., 2008; Chen et al., 2010; Zhu et al., 2015). Similar to such a typical design of a FSM, this paper uses the the two inch FSM depicted in Fig. 5, which can be rotated around x- and y-axes with a voltage driven voice coil motor actuation with an input range of $\pm 10V$.

For understanding the rotation dynamics of the FSM, one would typically have to model the dynamics of the FSM actuation system. Such a dynamic model must take into account the rotational inertia of the mirror, vibrations of the mirror/actuation system and possible dynamic coupling of vibrations due to off-centered actuation of the mirror positioning system. However, such dynamic information becomes readily available by performing experiments that reveal the coupled vibrations and static displacement of the mirror/actuation system in the form of step response excitation experiments.

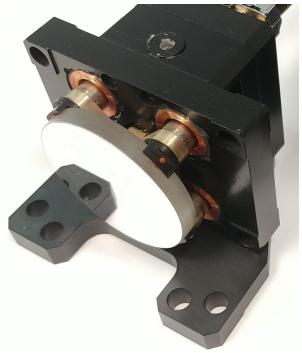

Fig. 5. FSM OIM202, courtesy of Optics in Motion LLC.

Discrete-time $k = 1, 2, \ldots$ data of mirror angle rotations $\alpha(k)$ and $\beta(k)$ due to the step response excitation of the VCMs of the FSM depicted in Fig. 5 are displayed in Fig. 6. During the experiments, independent Voltage step signals (block wave form signals) $V_\alpha(k)$ and $V_\beta(k)$ are applied to each of the VCM of the FSM, whereas multiple step response measurements are used for averaging and additional measurement noise reduction. It is worthwhile to note both the small, but non-negligible static and dynamic coupling between the rotation angle mirror angle rotations $\alpha(k)$ and $\beta(k)$.

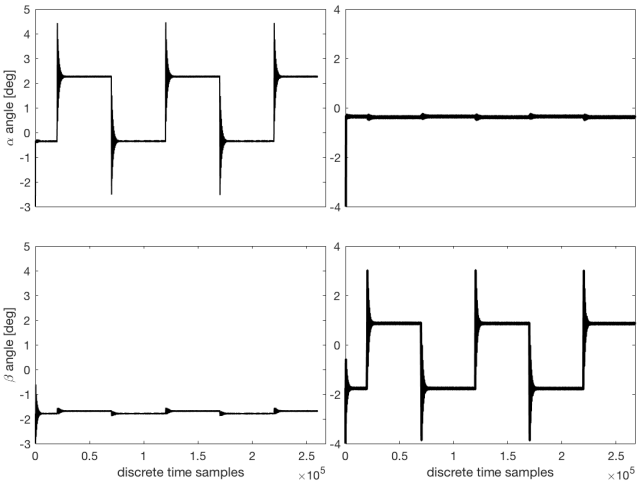

Fig. 6. Mirror step-response data. Left figures are $\alpha(t)$ and $\beta(t)$ angle rotation response to excitation of voltage $V_\alpha(t)$ of the voice coil motor (VCM) designed for α rotation. Right figures are the same angle rotation response to excitation of voltage $V_\beta(t)$ of the voice coil motor (VCM) designed for β rotation.

3.2 Step response realization

The process from step-response data to a linear dynamic model is accomplished with the step-response realization algorithm as presented in de Callafon and Miller (2012). The realization algorithm uses the averaged step response data in Fig. 6 to formulate a block Hankel matrix from which a fourth order multivariable discrete-time state-space model

$$x(k+1) = Ax(k) + B \begin{bmatrix} V_\alpha(k) \\ V_\beta(k) \end{bmatrix}, \quad \begin{bmatrix} \alpha(k) \\ \beta(k) \end{bmatrix} = Cx(k) \tag{11}$$

is derived via a singular value decomposition. More details of the procedure can be found in de Callafon and Miller (2012), as for this paper it suffices to conclude that the state-space model in (11) is able to model the static and dynamic coupling between the rotation angle mirror angle rotations $\alpha(t)$ and $\beta(t)$. A confirmation of the quality of the dynamic model is given in Fig. 7 that presents a visual comparison of the measured step response data and the simulated step response produced by the fourth order state space model in (11).

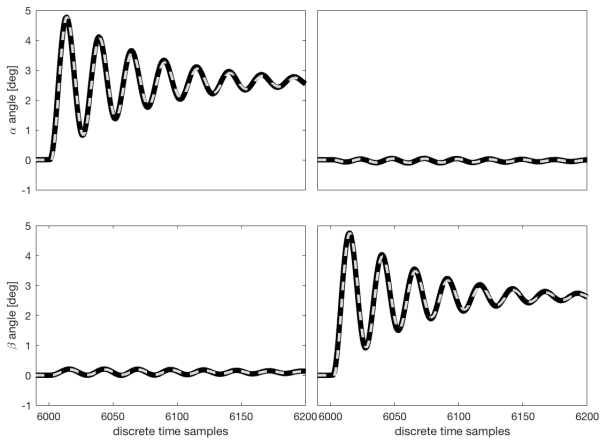

Fig. 7. Comparison between measured multivariable step response data (solid lines) and simulated multivariable step response data (dashed lines) obtained by fourth order state space model in (11) obtained, in turn, by the step response realization algorithm.

4. MIRROR INPUT SHAPING

4.1 Target parametrization

To illustrate the effectiveness of dynamic input shaping for a FSM, a target trajectory with fast dynamic transitions in the motion of the FSM is chosen. Without loss of generality we may assume a target surface aligned with the (y, z)-plane of the global coordinates and formulate fast dynamic transitions in form of a square trajectory as indicated in Fig. 8

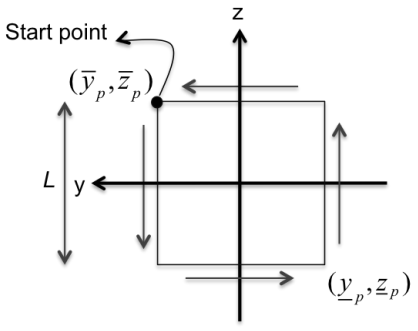

Fig. 8. Trajectory of the square of size L in target surface aligned in (y, z)-plane.

The trajectory is parametrized by a parameter ϕ by following the sequence from Fig. 8 according to

$$\begin{array}{lcl} (y_p(\phi), z_p(\phi))_1 & = & (\overline{y}_p, \overline{z}_p - \phi) \\ (y_p(\phi), z_p(\phi))_2 & = & (\overline{y}_p - \phi, \underline{z}_p) \\ (y_p(\phi), z_p(\phi))_3 & = & (\underline{y}_p, \underline{z}_p + \phi) \\ (y_p(\phi), z_p(\phi))_4 & = & (\underline{y}_p + \phi, \overline{z}_p) \end{array} \quad (12)$$
$$\text{for} \quad 0 \leq \phi \leq L$$

From the starting point $p = (\overline{y}_p(\phi), \overline{z}_p(\phi))$, we move through the axes by increments of ϕ, until we close the figure in the same starting point.

4.2 Inverse kinematics

Given a target trajectory $(y_p(\phi), z_p(\phi))$ parametrized in terms of ϕ by (12), the values for the desired mirror rotation pair $(\alpha(\phi), \beta(\phi))$ can be found by inverse kinematic analysis of the mirror rotation. In the inverse kinematic analysis, the mirror normal vector $n(\alpha, \beta)$ dependent reflection matrix $T(n(\alpha, \beta))$ given in (7) can be used to compute the desired mirror rotation pair $(\alpha(\phi), \beta(\phi))$.

To start the inverse kinematics process, we normalize the target p via

$$p_1(\phi) = \frac{p}{\|p\|}, \text{ where } p = (y_p(\phi), z_p(\phi))$$

and obtain the inverse direction vector p_1, towards the mirror. Having the direction of the incoming source beam p_0, we can obtain the normal of mirror $n(\phi)$ in the global coordinates as a function of the parameter ϕ via

$$n(\phi) = \frac{p_1(\phi) - p_0}{\|p_1(\phi) - p_0\|} \quad (13)$$

and the normal of the mirror in local coordinates given by

$$n_\ell(\alpha(\phi), \beta(\phi)) = R_y^{-1}(45^\circ) n_1(\phi).$$

Finally, the values of desired mirror rotation pair $(\alpha(\phi), \beta(\phi))$ are found by

$$\alpha(\phi) = \tan^{-1}\left(\frac{-n_\ell^y(\phi)}{n_\ell^z(\phi)}\right), \quad \beta(\phi) = \tan^{-1}\left(\frac{n_\ell^x(\phi)}{n_\ell^z(\phi)}\right) \quad (14)$$

by using (4), where n_ℓ^x indicates the x-coordinate, n_ℓ^y indicates the y-coordinate and n_ℓ^z indicates the z-coordinate of $n_\ell(\phi)$. Using the square shape as a target, we follow the inverse kinematics process to compute the angles sets $(\alpha(\phi), \beta(\phi))$ shown in Fig. 9, to reach the target as seen on Fig. 8.

4.3 Quasi-static input shaping

Reaching the desired target with the computed mirror angle pair $(\alpha(\phi(k)), \beta(\phi(k))$ obtained from the inverse kinematic analysis in (14) presents a challenge, as the actual FSM is a dynamic system. This challenge becomes apparent when a $(\alpha(\phi(k)), \beta(\phi(k))$ is required over a short time period $k = 1, 2, \ldots, N-1$ of $N = 300$ samples as depicted in Fig. 9 and leading to the target shape depicted in Fig. 10. It is clear that the dynamic behavior of the FSM interferes with the quasi-static analysis of the inverse kinematics.

4.4 Dynamic input shaping

To address the coupled static and dynamic motion of the FSM, input shaping is required. For the dynamic input shaping, knowledge of the dynamic model obtained by step

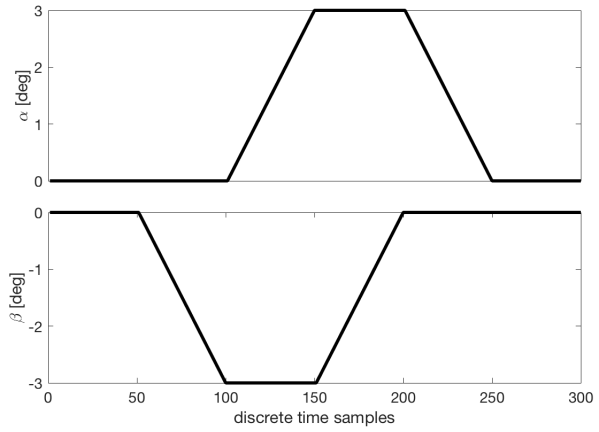

Fig. 9. Discrete-time mirror angle pair $\alpha(\phi(k))$ (top) and $\beta(\phi(k))$ (bottom) to obtain the desired target square of size L over a short time period of 300 samples.

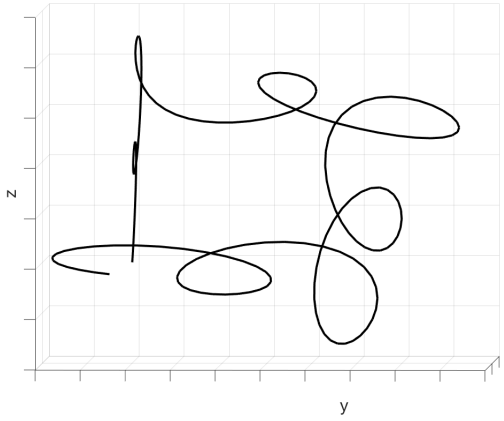

Fig. 10. Target shape produced by FSM due to VCM actuation scaled by computed quasi-static mirror angle pair $(\alpha(\phi(k)), \beta(\phi(k))$ of Fig. 9.

response experiments and given by the state space model in (11) can be used to constrain the dynamic motion of the FSM. For writing the (linear) motion constraints we follow an approach similar to Boettcher et al. (2010), but impose additional constraints on the desired static and dynamic motion of the FSM.

The first constraint is to enforce the resulting output $y(k) = [\alpha(k)\ \beta(k)]^T$ to be close to the desired output $y(\phi(k)) = [\alpha(\phi(k))\ \beta(\phi(k))]^T$ obtained from the inverse kinematic analysis in (14) via $y(k) \leq y(\phi(k)) + \varepsilon(k)$ and $y(k) \geq y(\phi(k)) - \varepsilon(k)$. Due to the dynamic behavior modeled by the state space model in (11) and under the assumption that initial state *x(1)=0*, such a constraint on the output $y(k)$ can be converted to the input $u(k) = [V_\alpha(k)\ V_\beta(k)]^T$ for input shaping at each time index $k = 1, 2, \ldots, N$ via the matrix relation $\mathbf{y} = \Phi\mathbf{u}$ with $\mathbf{y} = [y(1)\ y(2)\ \cdots\ y(N)]^T$, $\mathbf{u} = [u(1)\ u(2)\ \cdots\ u(N)]^T$ and

$$\Phi = \begin{bmatrix} 0 & 0 & \cdots & 0 \\ CB & 0 & \cdots & 0 \\ CAB & CB & \cdots & 0 \\ \vdots & \vdots & \vdots & \vdots \\ CA^{N-2}B & CA^{N-3}B & \cdots & 0 \end{bmatrix} \tag{15}$$

involving a lower Toeplitz matrix Φ with impulse response coefficients $CA^{k-2}B$. As a result, the first constraint is formulated as

$$\begin{matrix} \Phi\mathbf{u} \leq \mathbf{y}(\phi) + \varepsilon \\ -\Phi\mathbf{u} \leq -\mathbf{y}(\phi) + \varepsilon \end{matrix}, \varepsilon = \begin{bmatrix} \varepsilon(1) \\ \varepsilon(2) \\ \vdots \\ \varepsilon(N) \end{bmatrix}, \mathbf{y}(\phi) = \begin{bmatrix} y(\phi(1)) \\ y(\phi(2)) \\ \vdots \\ y(\phi(N)) \end{bmatrix} \tag{16}$$

with Φ defined in (15) and where ε is a desired accuracy of $\mathbf{y}$ from the desired output $\mathbf{y}(\phi)$ for each discrete-time interval k.

The next constraints impose constraints on the volatility and size of the resulting input signal $u(k) = [V_\alpha(k)\ V_\beta(k)]^T$. To avoid volatility in the voltage/input signals, constraints on the rate of change $|V_\alpha(k)(k) - V_\alpha(k)(k-1)| \leq d(k)$, $|V_\beta(k) - V_\beta(k-1)| \leq d(k)$ are implemented by

$$\begin{matrix} E\mathbf{u} \leq \mathbf{d} \\ -E\mathbf{u} \leq \mathbf{d} \end{matrix}, E = \begin{bmatrix} -1 & 0 & 1 & 0 & \cdots & 0 \\ 0 & -1 & 0 & 1 & \cdots & 0 \\ \vdots & & \ddots & \ddots & \ddots & \\ 0 & 0 & \cdots & -1 & 0 & 1 \end{bmatrix}, \mathbf{d} = \begin{bmatrix} d(1) \\ d(2) \\ \vdots \\ d(N) \end{bmatrix} \tag{17}$$

and constraints on the size of the input signal

$$\begin{matrix} \mathbf{u} \leq \bar{\mathbf{u}} \\ \mathbf{u} \geq \underline{\mathbf{u}} \end{matrix}, \ \bar{\mathbf{u}} = \begin{bmatrix} \bar{u}(1) \\ \bar{u}(2) \\ \vdots \\ \bar{u}(N) \end{bmatrix}, \ \underline{\mathbf{u}} = \begin{bmatrix} \underline{u}(1) \\ \underline{u}(2) \\ \vdots \\ \underline{u}(N) \end{bmatrix} \tag{18}$$

to avoid large values in the voltage/input signals during input shaping. As also observed in Boettcher et al. (2010) and Dautt-Silva and de Callafon (2018), the input shaping problem under the linear constraints of (16)-(18) can be written in a Linear Programming problem

$$\begin{matrix} \min\ \boldsymbol{f}^T\mathbf{u}, \text{ subject to} \\ [L\ -\mathbf{1}]\,\mathbf{u} \leq \mathbf{b} \\ \mathbf{u} \leq \bar{\mathbf{u}} \\ \mathbf{u} \geq \underline{\mathbf{u}} \end{matrix} \quad L = \begin{bmatrix} \Phi \\ -\Phi \\ E \\ -E \end{bmatrix}, \ \mathbf{b} = \begin{bmatrix} \mathbf{y}(\phi) + \varepsilon \\ -\mathbf{y}(\phi) + \varepsilon \\ \mathbf{d} \\ \mathbf{d} \end{bmatrix} \tag{19}$$

where **-1** is a column vector of ones with the same number or rows as L, and $\boldsymbol{f}$ is the coefficient vector, $\boldsymbol{f} = [0\ 0\ 0\ ...\ 1]$; for which a feasible solution must be found. Feasibility of a solution to (19) can be guaranteed by the choice of the margin ε or the bound on the rate of change $\mathbf{d}$. Although (19) does not provide a unique solution to the input shaped signal $\mathbf{u}$, lowering the allowable rate of change $\mathbf{d}$ will reduce the solution space.

Computation of a feasible solution to the LP problem of (19) using the target desired mirror rotation pair $y(\phi(k)) = [\alpha(\phi(k))\ \beta(\phi(k))]^T$ depicted earlier in Fig. 9 now leads to much better dynamic performance of the FSM in tracking the desired square trajectory. The results are summarized in Fig. 11 and it can be seen that despite the short period of $N = 300$ samples, the dynamics of the FSM is correctly handled by the input shaping routine.

It is also worthwhile to inspect the computed input shape $u(k) = [V_\alpha(k)\ V_\beta(k)]^T$ used as input for each of the VCM of the FSM. The input voltage signals are summarized in Fig. 12 and it is interesting to observe that the small changes in the input signal anticipate the both the static changes and vibrations of the FSM to reduce tracking errors and vibrations in the beam pointing.

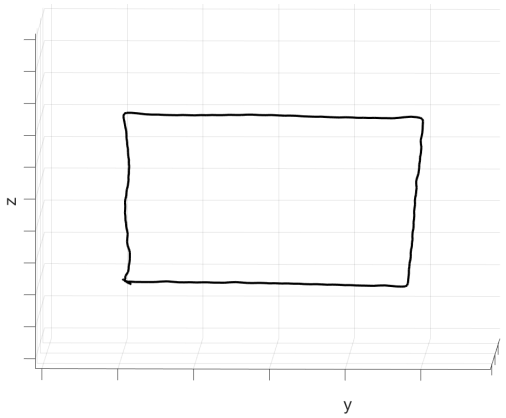

Fig. 11. Target shape produced by FSM due to VCM actuation via input shaping via Linear Programming problem (19).

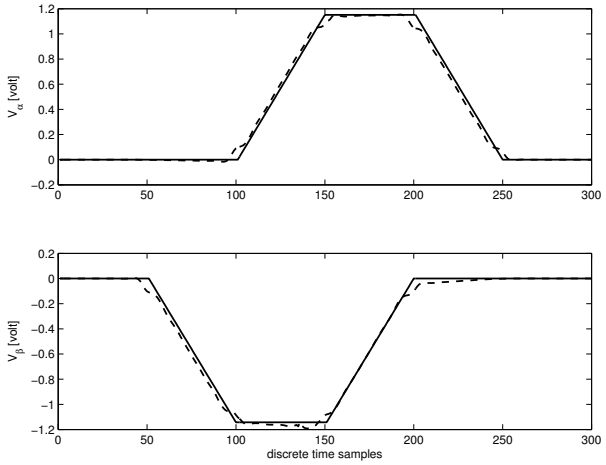

Fig. 12. Result of input shaping for $V_\alpha(k)$ (top) and $V_\beta(k)$ (bottom) with Comparison between the quasi-static input due to inverse kinematics only (solid lines) and the dynamic shaped input (dashed lines).

5. CONCLUSIONS AND FUTURE RESEARCH

Kinematic analysis and dynamic modeling based on step response experiments is shown to be an effective way to model both the quasi-static behavior of beam steering and the dynamic coupling of the motion system of a fast steering mirror (FSM). In case of a single FSM, inverse kinematic analysis can be used to compute desired mirror rotation angles. In addition, it has been shown that step response experiments can be used to formulate a multivariable model that captures both the static and dynamic coupling of a two-axis motion system of a FSM.

The work in this paper shows how desired mirror rotation angles and the multivariable model can be used to formulate an input shaping design that is solved via a standard Linear Programming problem. Experimental results from a commercial FSM are used to validate the approach and a comparison is made between standard quasi-static input and dynamically shaped input to show the effectiveness of the input shaping. Future work involves adding feedforward control to the input shaping, as well as creating an optical layout with feedback outside of the FSM, such as a position sensing device to measure and correct any error due to input shaping.

ACKNOWLEDGEMENTS

The authors acknowledge and thank Don Henderson from Optics in Motion LLC and Patrick Newton and Thomas Morrison for their support.

REFERENCES

Boettcher, U., de Callafon, R.A., and Talke, F.E. (2010). Multiobjective time domain input shaping for closed-loop discrete-time systems. In *Prepr. 5th IFAC Symposium on Mechatronic Systems*, 200–205. Cambridge, MA.

Chen, N., Potsaid, B., Wen, J.T., Barry, S., and Cable, A. (2010). Modeling and control of a fast steering mirror in imaging applications. *6th annual IEEE Conference on Automation Science and Engineering*, 27–32.

Dautt-Silva, A. and de Callafon, R.A. (2018). Optimal input shaping with finite resolution computed from step-response experimental data. In *Proc. American Control Conference*, 6703–6708.

de Callafon, R.A. and Miller, D.J. (2012). Identification of linear time-invariant systems via constrained step-based realization. In *Prepr. 16th IFAC Symposium on System Identification*, 1155–1160.

DeBruin, J.C. and Johnson, D.B. (1992). Line-of-sight reference frames: a unified approach to plane-mirror optical kinematics. *Proc. SPIE 1697, Acquisition, Tracking and Pointing VI*, 111–129.

Hilkert, J.M., Kanga, G., and Kinnear, K. (2014). Line-of-sight kinematics and corrections for fast-steering mirrors used in precision pointing and tracking systems. *Proc. SPIE 9076, Airborne Intelligence, Surveillance, Reconnaissance (ISR) Systems and Applications XI.*

Kim, B.S., Gibson, S., and Tsao, T.C. (2004). Adaptive control of a tilt mirror for laser beam steering. In *Proc. American Control Conference*, 3417–3421. Boston, Massachusetts.

Kim, K., Moon, S., Kim, J., and Lee, Y.P.J.H. (2019). Input shaping based on an experimental transfer function for an electrostatic microscanner in a quasistatic mode. *Micromachines*, 10. doi:10.3390/mi10040217.

Merritt, P. and Spencer, M. (2018). *Beam Control for Laser Systems.* Directed Energy Professional Society.

O'Rourke, J. (1998). *Computational Geometry in C.* Cambridge University Press.

Roggemann, M. and Welsh, B. (1996). *Imaging Through Turbulence.* CRC Press.

Schitter, G., Thurner, P., and Hansma, P. (2008). Design and input-shaping control of a novel scanner for high-speed atomic force microscopy. *Mechatronics.* doi: 10.1016/j.mechatronics.2008.02.007.

Zhou, Q., Ben-Tzvi, P., Fan, D., and Goldenberg, A.A. (2008). Design of fast steering mirror systems for precision laser beams steering. *ROSE 2008 IEEE International Workshop on Robotic and Sensors Environments.*

Zhu, W., Bian, L., An, Y., Chen, G., and Rui, X. (2015). Modeling and control of a two-axis fast steering mirror with piezoelectric stack actuators for laser beam tracking. *Smart Materials and Structures*, 27. doi: 10.1088/0964-1726/24/7/075014.